https://doi.org/10.18321/ectj705

Numerical Simulation of Turbulent Flames based on a Hybrid RANS/Transported-PDF Method and REDIM Method

C. Yu[1*], F. Minuzzi[2], U. Maas[1]

[1]Institute of Technical Thermodynamics, Karlsruhe Institute of Technology, Germany
[2]Graduate Program in Applied Mathematics, Federal University of Rio Grande do Sul, Brazil

Article info

Received:
10 May 2017

Received in revised form:
16 July 2017

Accepted:
25 October 2017

Abstract

A hybrid RANS/Transported-PDF model for the simulation of turbulent reacting flows based on automatically reduced mechanisms for the chemical kinetics (reaction-diffusion manifold, REDIM) is presented in this work. For modelling of turbulent reacting flows, chemistry is a key problem and affects largely the accuracy. The PDF method has been widely used since the chemical source term is in a closed form, without any modelling. Despite of this advantage of PDF method, detailed chemical kinetics is not desired due to its heavy computational effort. From this aspect, the detailed chemical kinetics is simplified by the reaction-diffusion manifold (REDIM) method. The hybrid RANS/Transported-PDF model based on REDIM reduced kinetics is applied to simulate the Sandia piloted Flame E, which has a moderate degree of local extinction. The numerical results are validated through comparison with experimental data and show good qualitative and quantitative agreements.

1. Introduction

Numerical modelling of turbulent combustion is based on the solution of the governing conservation equations for mass, species, momentum and energy. Direct numerical simulations (DNS) are the most fundamental approach to solve the Navier-Stokes (N-S) equations. It resolves all the turbulent length scales with initial and boundary conditions appropriate to the flow considered [1]. Conceptually DNS is the simplest approach without introducing any models. However, its computational cost increases rapidly with increasing Reynolds number, so that its applicability is restricted to low to moderate Reynolds numbers [1, 2]. Due to this limitation of DNS, several techniques requiring modelling are developed and their computational requirements are much less than DNS. One technique is Large-eddy simulation (LES) which solves relative large turbulent length scales and the smaller-scale motions are solved by applying models [1, 3]. Another technique is solving Reynolds-averaged N-S equations (RANS) [1].

For turbulent reacting flow problems, turbulence and chemistry have a strong interaction and the simulation of this interaction is quite complicated. One of the challenges is to simulate or model chemical source terms, since they are influenced by turbulent mixing, molecular transport and chemical kinetics. Most of the earlier developed models such as Eddy-break-up (EBU) model [4], k-ε-g model [5] and equilibrium-chemistry-assumption model [2] are based on certain assumptions such as infinite fast reaction rate. Hence, these models cannot predict complicated reacting flows with ignition, extinction and problems with slow reactions (NO_x, soot, etc.).

The probability density function (PDF) model can overcome the complexity of solving the chemical source term. In the transported-PDF equation, the chemical source term appears in a closed form, avoiding any modelling [6, 7]. Furthermore, by solving the transported-PDF equation, the PDF of velocity and thermo-kinetics scalars and, consequently, their average values and statistical moments of any order can be obtained.

*Corresponding author. E-mail: chunkan.yu@kit.edu

To reduce the computational effort, reduced kinetic models are needed. Usually, characteristic time scales for a combustion system differ by orders of magnitude from 1 s to 10^{-10} s [8, 9]. Such multiple scales cause the existence of low-dimensional manifolds of slow and fast dynamic motions imbedded into the whole composition space [8]. Accordingly, the whole state space vector can be recovered by using the low manifold and the main task is to find out thus low manifold in the state space that can be used to approximate the full system dynamics. In this work, the reaction-diffusion manifold (REDIM) reduction method [10], which takes physical transportation into account, is applied to simplify the chemical kinetics, whose whole evolution is continued to a manifold with a much lower dimension.

In this work, a hybrid RANS/transported-PDF model is discussed and applied. Furthermore the REDIM as reduced chemical kinetics is used. Simulations based on RANS/PDF method and REDIM reduced chemistry are performed for the famous Sandia piloted Flame E, which represents moderate degree of local extinction.

2. Hybrid RANS/Transported-PDF Model

The numerical method used in this work is a hybrid RANS/Transported-PDF model. This model consists of two parts: one is the RANS providing the hydrodynamic quantities; the other is the transported-PDF equation providing the thermo-kinetic state of the flow. The principles of both models will be overviewed and their coupling briefly discussed.

2.1 RANS model

In the RANS model the favre-averaged conservation equations for mass and momentum are solved. The conservation equation for energy needs not to be solved, since the favre-averaged temperature $\tilde{T}$ is determined in the PDF part from the thermos-kinetic state of the fluid [11, 12]. Consequently, the averaged ideal gas law

$$\bar{p} = \bar{\rho} \cdot \widetilde{R_g T}, \tag{1}$$

together with conservation equations, are solved simultaneously to obtain the mean velocities.

The unclosed terms of Reynolds stresses, $\overline{\rho u_i'' u_j''}$ is obtained from the PDF part, as indicated in Fig. 1 (discussed later).

2.2. PDF model

A joint PDF (JPDF) of velocity, composition and turbulent frequency $\boldsymbol{f}_{\omega U\phi}$ (Θ, $\boldsymbol{V}$, $\boldsymbol{\psi}$; $\boldsymbol{x}$, t) is employed here. This is a one-point, one-time joint PDF which has the main advantage to treat chemical reaction exact without any modelling assumptions [6, 7].

A transported-PDF equation is solved to obtain the PDF, which overcomes the problem that generally the PDF of a flow is a priori unknown. This transported-PDF equation for $\boldsymbol{f}_{\omega U\phi}$ (Θ, $\boldsymbol{V}$, $\boldsymbol{\psi}$; $\boldsymbol{x}$, $\boldsymbol{t}$) reads [6, 7]:

$$\begin{aligned}
&\rho(\boldsymbol{\psi})\frac{\partial f}{\partial t} + \rho(\boldsymbol{\psi})V_i\frac{\partial f}{\partial x_i} - \frac{\partial \bar{p}}{\partial x_i}\frac{\partial f}{\partial V_i} + \frac{\partial \rho(\boldsymbol{\psi})S_\alpha(\boldsymbol{\psi})f}{\partial \psi_\alpha} \\
&= -\frac{\partial}{\partial V_i}\left(\overline{\left.\frac{\partial \tau_{ij}'}{\partial x_j} - \frac{\partial p'}{\partial x_i}\right| \Theta, \boldsymbol{V}, \boldsymbol{\psi}}\right)\cdot f \\
&\quad + \frac{\partial}{\partial \psi_\alpha}\left(\overline{\left.\frac{\partial J_{\alpha,i}'}{\partial x_i}\right| \Theta, \boldsymbol{V}, \boldsymbol{\psi}}\right)\cdot f - \frac{\partial}{\partial \theta}\left(\overline{\left.\frac{\mathrm{D}\omega}{\mathrm{D}t}\right| \Theta, \boldsymbol{V}, \boldsymbol{\psi}}\right)\cdot f,
\end{aligned} \tag{2}$$

where S_α (ψ) denotes the chemical source term, D/Dt denotes to the material derivative and J_α the diffusion flux density. In (2) the mean viscous stress $\bar{J}_\alpha$ and the mean diffusion $\bar{\tau}_{ij}$ are neglected because both terms are of little importance for flows with high Reynolds numbers. It can be observed that all terms on the left-hand side are in a closed form, including the chemical source term $S_\alpha(\psi)$. However, all the conditional terms on the right-hand side are unclosed and must be modelled.

The numerical integration of transported-PDF equation is performed using a particle method. The evolution of the composition vector can be calculated as

$$\frac{\mathrm{d}\boldsymbol{\phi}^{*,i}}{\mathrm{d}t} = \boldsymbol{S}\left(\boldsymbol{\phi}^{*,i}\right) + \boldsymbol{M}\left(\boldsymbol{\phi}^{*,i}, \ldots, \boldsymbol{\phi}^{*,Np}\right), i = 1,2, \ldots, N_p \tag{3}$$

in which N_p is the number of particles per cell. $S(\phi^*)$ is calculated from a lookup table generated based on REDIM method, an automatic reduction method of detailed chemical mechanisms. M is the effect of molecular mixing process. For more detailed numerical method readers may refer to [6, 7].

2.3. Coupling of RANS and transported-PDF model

The coupling between the RANS model and the transported-PDF model is represented in Fig. 1. The Reynolds stresses $\overline{\rho u_i'' u_j''}$ and the favre-averaged temperature $\widetilde{R_g T}$ are calculated through

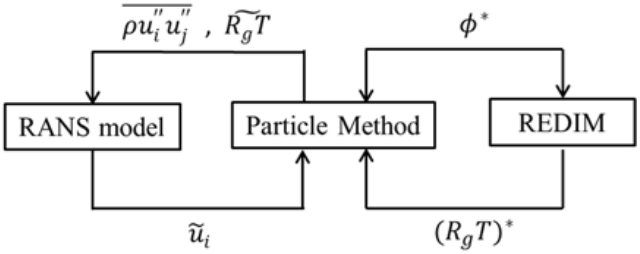

Fig. 1. Overview of coupling between RANS and transported-PDF model (particle method) based on REDIM.

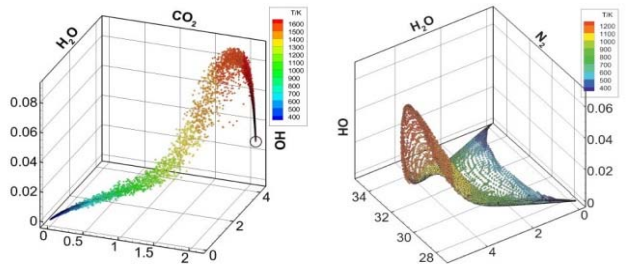

Fig. 2. Distribution of composition states from DNS in 3D projection of composition state space. Unit of specific mole number is [ϕ] = mol/kg.
Figure is taken from [13] under permission of author.

the particle method and serve as known quantities for the favre-averaged conservation equations for mass and momentum. The RANS model determines the favre-averaged velocity, used in particle method to obtain the particle position, velocity and turbulent frequency.

The reduced chemical kinetics of particles ϕ^* is solved by using (3), which determine the temperature of particles$(R_gT)^*$ and the favre-averaged temperature $\widetilde{R_gT}$ as well.

3. Reduced chemical kinetics: Reaction-Diffusion Manifolds (REDIM)

For practical applications, a complete solution of the governing species conservation equations including detailed chemical kinetics is impossible because reaction mechanisms always involve a large number of chemical species and reaction steps [9].

However, one can observe that the whole dynamic system can be approximately described by a much lower dimensional manifold, which is shown in Fig. 2. In Fig. 2 two DNS results of premixed turbulent methane-air-flame (left) [13] (DNS data taken from [14]) and non-premixed hydrogen-air counter-flow flame (right) [13] (adapted from [15]) in a 3D projection of state space are shown. We observe clearly a low-dimensional structure and the reason for such structure is that there exist different characteristic time scales describing chemical and physical process in combustion systems [8]. Following this observation, the manifold based reduced kinetics was developed to find out this low-dimensional manifold which reduces both the stiffness and the dimension of the governing species conservation equations.

In this work, the reduction method of chemical kinetics, Reaction-diffusion manifolds (REDIM) [10], is applied to reduce both the dimensionality and stiffness of the PDE systems to be integrated in the numerical simulation. In REDIM it decouples the fast and slow processes automatically accounting for the coupling with physical transports. It is because of the existence of fast timescales that the whole evolution of chemical kinetics is governed by an invariant manifold with a much lower dimension defined as:

$$\mathcal{M} = \{\boldsymbol{\Psi}: \boldsymbol{\Psi} = \boldsymbol{\Psi}(\boldsymbol{\theta}),\ \boldsymbol{\Psi}: R^m \to R^n\}, \qquad (4)$$

in which m is the dimension of reduced chemical kinetics, n the dimension of detailed chemical kinetics, $\boldsymbol{\Psi}$ the original full n-dimensional state vector and $\boldsymbol{\theta}$ the m-dimensional vector of reduced coordinates.

As proposed in [10], the invariance condition for the slow manifold used in REDIM is:

$$\mathbf{0} = (\mathbf{I} - \boldsymbol{\Psi}_{\boldsymbol{\theta}} \boldsymbol{\Psi}_{\boldsymbol{\theta}}^{+}) \cdot \boldsymbol{\Phi}(\boldsymbol{\Psi}(\boldsymbol{\theta})), \qquad (5)$$

where $\boldsymbol{\Phi}$ $(\boldsymbol{\Psi}(\boldsymbol{\theta}))$ is the sum of source term, convection term and diffusion term and $\boldsymbol{\Psi}_{\theta}^{+}$ is the Moore-Penrose pseudo-inverse of $\boldsymbol{\Psi}_{\theta}$.

To find out the solution of (5), it is suggested to solve the corresponding evolution equation:

$$\frac{\partial \boldsymbol{\Psi}(\boldsymbol{\theta})}{\partial t} = (\mathbf{I} - \boldsymbol{\Psi}_{\boldsymbol{\theta}} \boldsymbol{\Psi}_{\boldsymbol{\theta}}^{+}) \cdot \boldsymbol{\Phi}(\boldsymbol{\Psi}(\boldsymbol{\theta})), \qquad (6)$$

until the stationary solution of (6) reaches, yielding the desired REDIM manifold defined in (5).

4. Numerical Setup

4.1. Test Case

To validate the hybrid RANS/Transported-PDF method with REDIM reduced chemistry, the Sandia piloted Flame E [16] is considered. A fuel jet with diameter D = 7.2 mm consists of 25% methane and 75% air. The jet is surrounded by a coaxial

pilot flame, which is operated lean. For Flame E the Reynold number of jet is 33600, corresponding to a jet velocity of 74.4 m/s. Due to its relative high Reynold number, a moderate degree of local extinction and re-ignition can be observed [16, 17].

4.2. Numerical method for RANS/Transported-PDF method

The equations of the RANS models are solved by using the CFD code SPARC [18]. It is based on a finite volume method to solve the compressible RANS equations on block structured domains. For our test case, a cylindrical coordinate system (x, r) is used, where x is the downstream direction and r the radial direction.

The transported-PDF Eq. (2) is solved by using a Monte-Carlo particle method, because the numerical effort increases only linear with the number of dimensions [6, 7]. In this particle method, a set of stochastic differential equations (SDE) are solved for the evolution of notional particles. The position of each notional particle is evolved by its own velocity. The evolution of its velocity is modeled by the simplified Langevin model (SLM) [1]. The turbulent frequency is modeled based on the gamma-distribution model [1]. The mixing process in (3) is modeled by using the modified Curl's model (MCM) [19]. It should be emphasized here that the mixing model has a large effect on the accuracy of simulation results [20]. In the MCM, pairs of particles within the same cell are randomly selected and mixed with certain mixing intensity. Even though the MCM is one of the classical methods for the modeling of mixing process, it has some shortcomings such as non-localness in physical and composition space [21], resulting in discontinuous jump processes. One advanced method to overcome this problem is the multiple mapping conditioning (MMC) [22]. In MMC pairs of particles are so selected that both are close in physical and composition space. The MMC has also been successfully applied in our previous study [12], but here we focus on the MCM model only.

In Table 1, parameters and their values and corresponding applied models in PDF method are listed. For more detailed explanation, please refer to e.g. [1, 6]. In this work, radiation is not considered.

For the computational simulation, a domain with $120D_j \times 40D_j$ is used and discretized by 51 cells in x direction and 42 cells in r direction (total 2142 cells in computational domain). The numerical simulation is started with 50 particles per cell.

Table 1
Overview of parameters and their values and corresponding applied models in PDF method

Parameter	Value	Applied Model
C_0	2.1	Simplified Langevin Model
C_Ω	0.6893	Turbulent Frequency Model
$C_{\omega 1}$	0.71	
$C_{\omega 2}$	0.9	
C_3	1.0	
C_4	1.25	
C_ϕ	2.8	Mixing model

A particle number control is also applied [21]. The maximal particle number within one cell is allowed to be 60, and the minimal to be 40.

4.3. REDIM reduced chemistry and its validation in case of laminar flames

To get the REDIM reduced chemistry, one must solve (6), until the stationary solution is obtained. In order to solve it numerically, one needs the initial conditions. In principle one can use any initial profiles, since one is only interested in the stationary solution of (6) [10]. However, since the initial profiles also define the boundary/ applicable region of REDIM reduced chemistry, the configurations important for Sandia Flame are considered.

For Sandia Flame, one has three different states: (i) jet, (ii) pilot and (iii) air. Therefore, the initial profiles consist of the following 4 configurations: (i) jet-pilot laminar counter-flow diffusion flame, (ii) pilot-air laminar counter-flow diffusion flame, (iii) jet-air laminar counter-flow diffusion flame and (iv) pure mixing between jet and air. For (i), (ii) and (iii) configurations, one calculates the laminar counter-flow diffusion flame with different stretch rate. The profiles are calculated by using INSFLA [23, 24] and GRI 3.0 [25] as detailed mechanism. In the calculation, unity Lewis number ($Le = 1$) is considered.

In Fig. 3 several important laminar flamelets are shown. Blue and brown lines are the configuration of jet-pilot and pilot-air laminar counter-flow diffusion flame, together yielding the upper boundary of REDIM. Red lines represent the configuration of jet-air laminar counter-flow diffusion flames with the lowest (upper red line) and highest (lower red line) stretch rate used in the initial profile. The cyan line stands for the configuration of pure mixing between jet and air, defining the lower boundary of REDIM.

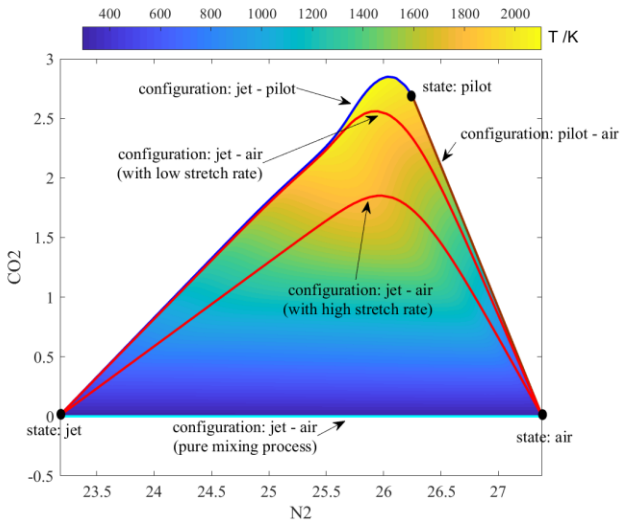

Fig. 3. Contour plot of temperature as a function of specific molar number of N_2 and CO_2 in REDIM. Black full points: different states for Sandia Flame. Colored lines: different critical flamelets of laminar counter-flow diffusion flames. Unit of specific mole number is $[\phi]$ = mol/kg.

The progress variables used here are specific mole numbers of CO_2 (ϕ_{CO_2}) and N_2 (ϕ_{N_2}), consistent to the situation in previous study [11, 12]. That means, a 2-dimensional (2D) REDIM is used. In Fig. 3 the contour plot of temperature as a function of progress variables N_2 and CO_2 in REDIM is also shown. Note that in REDIM all the thermo-chemical quantities such as enthalpy, mixture fraction and mass fractions of species are functions of N_2 and CO_2.

An interesting question is, whether the REDIM reduced chemistry can describe the flame extinction phenomenon, since for the establishment of REDIM no a-priori information about flame extinction is required. In Fig. 4 the REDIM reduced chemistry is compared with quenching flamelets in N_2-CO_2-OH projection for the configuration of jet-air laminar counter-flow diffusion flame. The blue line is the stationary initial flamelet and green lines are transient quenching flamelets. It can be observed that the REDIM reduced chemistry (red mesh grid) and the green flamelets "almost" overlap, so that REDIM can describe the flame extinction process quite well.

To validate the 2D REDIM reduced chemistry, a numerical simulation for jet-air counter-flow diffusion flame, one of the configurations in Sandia Flame, is conducted and compared with results based on detailed chemistry, which is shown in Fig. 5. Shown in figure are the temperature and mass fractions of O_2, OH and NO over specific molar

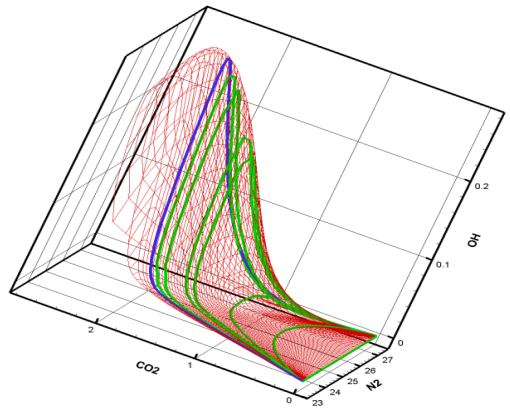

Fig. 4. Comparison of REDIM (red mesh grid) with flamelets describing flame extinction of configuration jet-air laminar counter-flow diffusion flame (solid lines) in N_2-CO_2-OH projection.

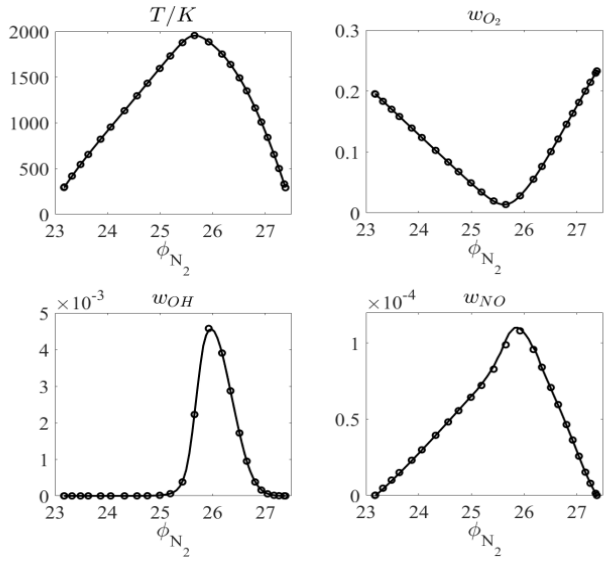

Fig. 5. Comparison of temperature, mass fractions of O_2, OH and NO over specific molar number of N_2 (ϕ_{N_2}) for jet-air counter-flow diffusion flame. Circles: using detailed chemistry. Lines: using 2D REDIM reduced chemistry. Unit of specific mole number is $[\phi]$ = mol/kg.

number of N_2 (ϕ_{N_2}). It can be clearly observed that the results based on 2D REDIM reduced chemistry (lines) agree with those based on detailed chemistry (circle) very well for all four quantities.

5. Results and discussions

To validate the hybrid RANS/Transported-PDF method with REDIM reduced chemistry, the simulation results will be compared with experimental data for Sandia piloted Flame E [16]. The experimental data can be downloaded from [17]. Note that the dimensionless mixture fraction is determined according to the Bilger expression, which

is consistent to the definition used in the experimental evaluation [16, 17]. In the following, all favre-averaged quantities are written with tilde such as favre-averaged temperature $\tilde{T}$ or favre-averaged mass fraction $\widetilde{w}$.

Figure 6 shows the profiles of temperature and mass fractions of CH_4, OH and CO over mixture fraction along the centerline of main jet (r = 0 mm) plotted together with experimental data [17]. We see that the simulation results agree very well with the experimental data, although a slight deviation of CO in peak value can be observed. This may be caused by the uncertainty in the measurement or in the reaction mechanisms applied.

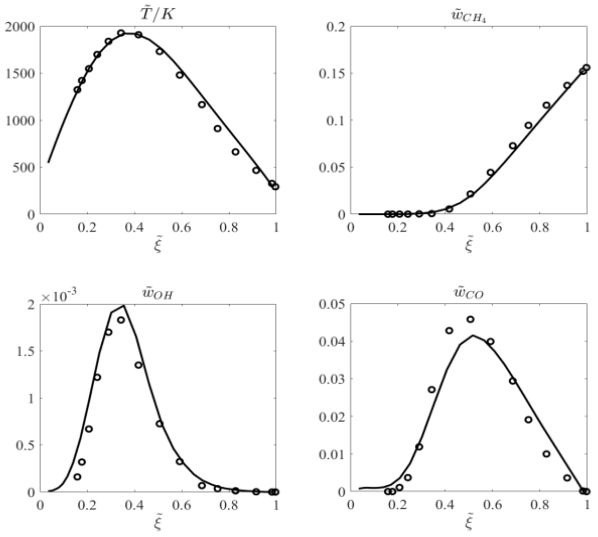

Fig. 6. Profiles of temperature and mass fractions of CH_4, CO and OH over mixture fraction along the centerline of main jet (r = 0 mm). Circles: experimental measurement [17]; Lines: simulation results.

Figure 7 shows the radial profiles of mean and rms of mixture fractions at four different locations. One can observe that the simulation results are in good agreement with the experimental data at all locations. The only noticeable deviation occurs at the peak values for rms of mixture fractions. The simulation results under-predicts the peak values, which may be caused by the mixing model. It was already shown that using other more advanced mixing models with optimal mixing model parameter can predict these peak values much better [20].

In Figs. 8–10, the conditional means of temperatures (Fig. 8) and mass fractions of CO (Fig. 9) and OH (Fig. 10) are compared at four different locations to the experimental data. It can be observed from Fig. 8 that the conditional mean temperatures are slightly over-predicted at rich region for x/D_j = 7.5 and 15 and agree very well for x/D_j = 30 and 45. From Fig. 9 the conditional mean mass fractions of CO agree well with experimental data under lean to stoichiometric conditions, while under rich conditions they are largely over-predicted for x/D_j = 7.5 and 15 and under-predicted for x/D_j = 30 and 45. The least convincing agreement is for mean mass fraction of OH in Fig. 10, for which the maximum over-prediction of the peak value is about 50% (at x/D_j = 7.5). Similar observations are also obtained in [26, 27]. It is believed that the under-/over-prediction of CO and OH under rich conditions can be attributed to the mechanism.

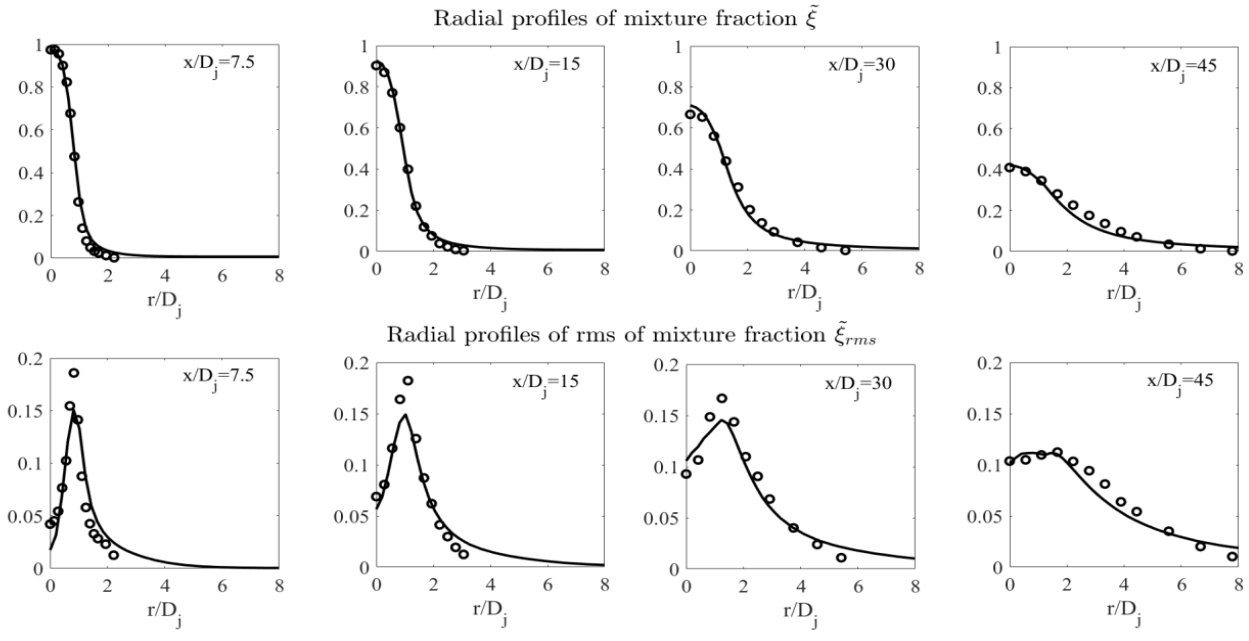

Fig. 7. Radial profiles of mean and root mean square (rms) of mixture fraction at x/D_j = 7.5, 15, 30 and 45. Circles: experimental measurement [17]; Lines: simulation results.

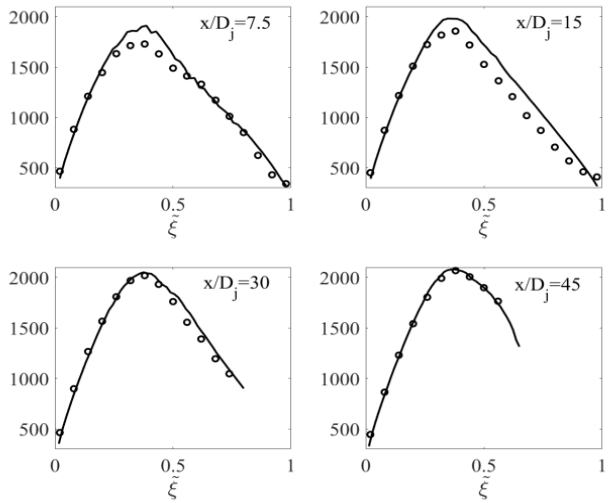

Fig. 8. Conditional temperature $\widetilde{T|\xi}$ at x/D_j = 7.5, 15, 30 and 45. Circles: experimental measurement [17]; Lines: simulation results.

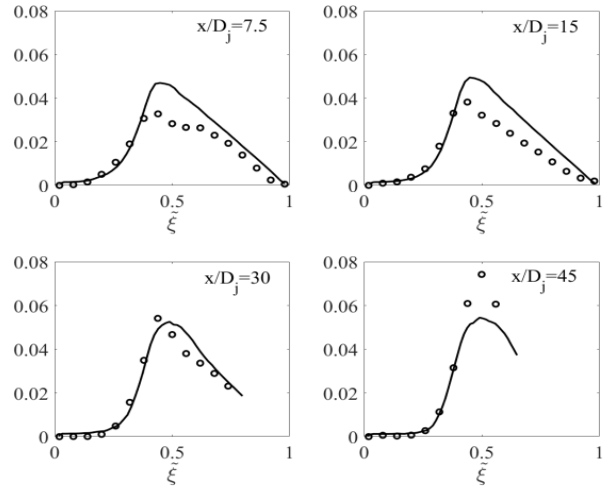

Fig. 9. Conditional mass fraction of CO $w_{CO}|\xi$ at x/D_j = 7.5, 15, 30 and 45. Circles: experimental measurement [17]; Lines: simulation results.

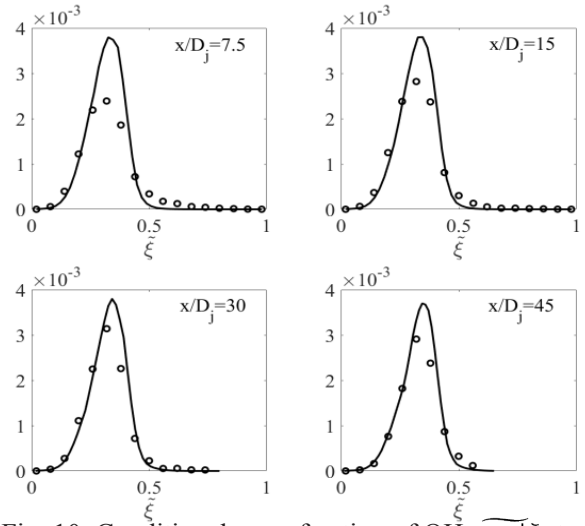

Fig. 10. Conditional mass fraction of OH $\widetilde{w_{OH}|\xi}$ at x/D_j = 7.5, 15, 30 and 45. Circles: experimental measurement [17]; Lines: simulation results.

In Fig. 11, scatter plots of temperature and mass fraction of OH over mixture fraction at x/D_j = 15 are compared with experimental measurement [17]. We notice that the proposed method based on REDIM can capture the local extinction (low values of mass fraction of OH), even though the degree of local extinction is still under-predicted. Note that better scatter plots can be achieved using more accurate turbulence model such as large eddy simulation (LES) [28].

In Figs. 12–14, the PDF of temperatures at x/D_j = 7.5 (Fig. 12), x/D_j = 15 (Fig. 13) and x/D_j = 30 (Fig. 14) for the corresponding four different radiuses from experiment (black bars) and simulation (blue bars) are plotted together and compared with each other. It can be observed that the simulation results agree with experimental data very well.

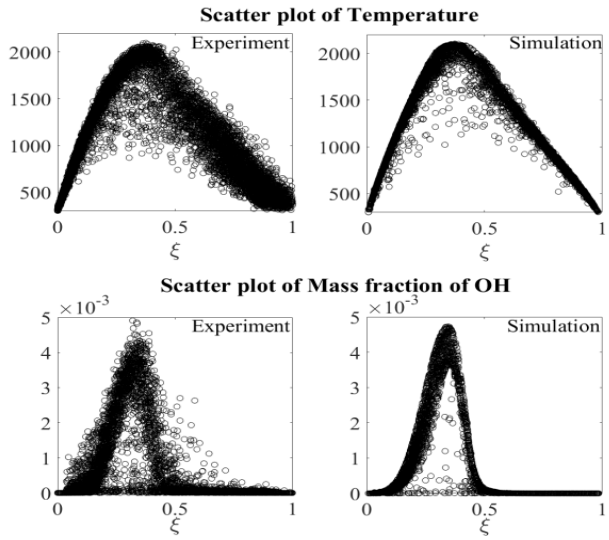

Fig. 11. Scatter plots of temperature and mass fraction of OH over mixture fraction at x/D_j = 15. Left: experimental measurement [17]; Right: simulation results.

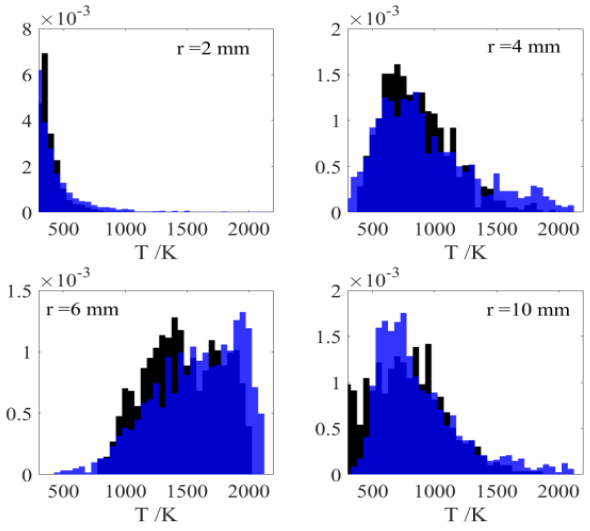

Fig. 12. PDF of temperatures at x/D_j = 7.5 for four different radiuses. Black bars: experimental measurement [17]; Blue bars: simulation results.

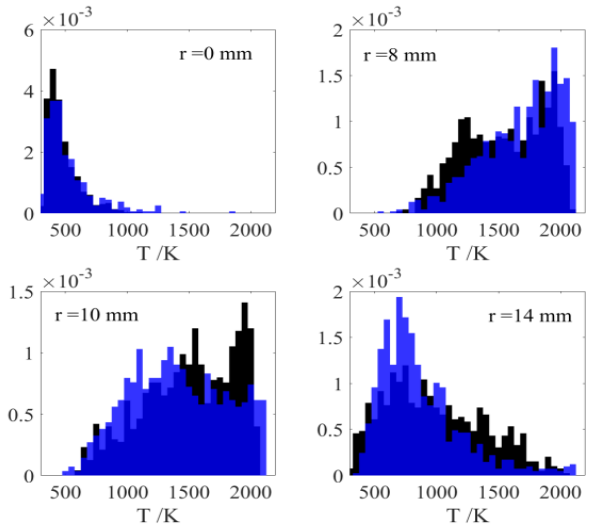

Fig. 13. PDF of temperatures at $x/D_j = 15$ for four different radiuses. Black bars: experimental measurement [17]; Blue bars: simulation results.

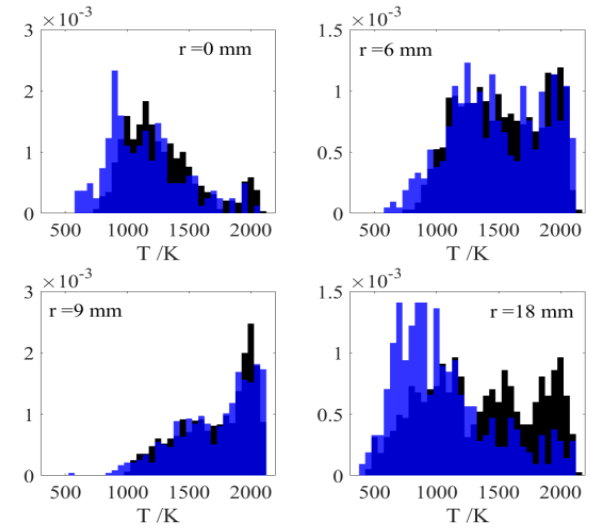

Fig. 14. PDF of temperatures at $x/D_j = 30$ for four different radiuses. Black bars: experimental measurement [17]; Blue bars: simulation results.

6. Conclusions

In this work, a hybrid RANS/transported-PDF model based on 2D REDIM as reduced chemical kinetics for the simulation of turbulent reacting flows is presented and validated. The reduced chemical kinetics, REDIM, allows an accurate modelling with only a small number of parameters (2 parameters in this work), which already account for the effect of molecular transport in the composition space. Using the REDIM reduced chemical kinetics largely reduces the computational simulation time.

The hybrid RANS/transported-PDF model based on REDIM is validated through one well-known flame: Sandia piloted Flame E, which represents moderate degree of local extinction due to its high Reynolds number. It is shown that simulation results have very good agreement with experimental data, except for the conditional favre-averaged mass fraction of CO and OH under rich conditions.

Including a radiation model with coupling of REDIM reduced chemistry will be subject of further work.

7. Acknowledgements

Financial supported by the German Research Foundation (DFG) within the project SFB/TR150 is gratefully acknowledged. Felipe Minuzzi is supported by CAPES – Coordination for the Improvement of Higher Education Personnel – Brazil, under the grant No. 88881.132868/2016-01.

References

[1]. S.B. Pope, Turbulent Flows, Cambridge University Press, Cambridge, U.K., 2000, 771 pp.

[2]. J. Warnatz, U. Maas and R.W. Dibble, Combustion: Physical and Chemical Fundamentals, Modeling and Simulation, Experiments, Pollutant Formation, Berlin: Springer-Verlag, 2000.

[3]. J. Fröhlich, Large eddy simulation turbulenter Strömungen, Wiesbaden: Teubner, 2006.

[4]. D. Spalding, *Symp. (Int.) Combust.* 13 (1971) 649–657. DOI:10.1016/S0082-0784(71)80067-X

[5]. D. Spalding, *Chem. Eng. Sci*. 26 (1) (1971) 95–107. DOI: 10.1016/0009-2509(71)86083-9

[6]. S.B. Pope, *Prog. Energ. Combust.* 11 (2) (1985) 119–192. DOI: 10.1016/0360-1285(85)90002-4

[7]. D.C. Haworth, *Prog. Energ. Combust.* 36 (2) (2010) 168–259. DOI: 10.1016/j.pecs.2009.09.003

[8]. U. Maas and S.B. Pope, *Combust. Flame* 88 (3) (1992) 239–264. DOI: 10.1016/0010-2180(92)90034-M

[9]. T. Turanyi and A. S. Tomlin, Analysis of Kinetic Reaction Mechanisms, Springer, 2014. DOI: 10.1007/978-3-662-44562-4

[10]. V. Bykov and U. Maas, *Combust. Theor. Model.* 11 (6) (2007) 839–862. DOI: 10.1080/13647830701242531

[11]. G. Steinhilber, Numerische Simulation turbulenter Verbrennungsprozesse mittels statistischer Verfahren und REDIM reduzierter

Kinetik, Dissertation Karlsruhe: Karlsruhe Institute of Technology, 2015.
[12]. C. Yu and U. Maas, "A hybrid RANS/ Transported-PDF Model for Simulation of Turbulent Flames based on generalized MMC and REDIM Method," in Proc. 8th European Combustion Meeting, Dubrovnik, Croatia, April 18 - April 25, 2017.
[13]. A. Neagos, Adaptive Generierung von Reaktions-Diffusions-Mannigfaltigkeiten für die reduzierte Beschreibung chemisch reagierender Strömungen, Diss. Dissertation, Karlsruhe, Karlsruher Institut für Technologie (KIT), 2017.
[14]. H. Carlsson, R. Yu and X.-S. Bai, *Int. J. Hydrogen Energ.* 39 (35) (2014) 20216–20232. DOI: 10.1016/j.ijhydene.2014.09.173
[15]. R. Schießl, V. Bykov, U. Maas, A. Abdelsamie and D. Thévenin, *P. Combust. Inst.* 36 (1) (2017) 673–679. DOI: 10.1016/j.proci.2016.07.089
[16]. R. Barlow and J. Frank, *Symp. (Int.) Combust.* 27 (1998) 1087–1095. DOI: 10.1016/S0082-0784(98)80510-9
[17]. "International workshop on measurement and computation of turbulent nonpremixed flames," [Online]. Available: http://www.sandia.gov/TNF/abstract.html. [Accessed 18 09 2014].
[18]. F. Magagnato, "SPARC: Structured Parallel Research Code," Task Quarterly 2.2, pp. 215–270, 1998.
[19]. J. Janicka, W. Kolbe and W. Kollmann, *J. Non-Equilib. Thermodyn.* 4 (1) (1979) 47–66. DOI: 10.1515/jnet.1979.4.1.47
[20]. R.R. Cao, H. Wang and S.B. Pope, *P. Combust. Inst.* 31 (2007) 1543–1550. DOI: 10.1016/j.proci.2006.08.052
[21]. R.O. Fox, Computational models for turbulent reacting flows, Cambridge University Press, 2003. DOI: 10.1017/CBO9780511610103
[22]. M.J. Cleary and A.Y. Klimenko, *Flow, Turbulence and Combustion* 82 (2009) 477–491. DOI: 10.1007/s10494-008-9161-3
[23]. U. Maas, Mathematische Modellierung instationärer Verbrennungsprozesse unter Verwendung detaillierter Reaktionsmechanismen, Dissertation, Ruprecht-Karls-Universität Heidelberg, 1988.
[24]. U. Maas and J. Warnatz, *Combust. Flame* 74 (1988) 53–69. DOI: 10.1016/0010-2180(88)90086-7
[25]. "GRI-Mech Home Page," [Online]. Available: http://www.me.berkeley.edu/gri_mech/.
[26]. J. Xu and S.B. Pope, *Combust. Flame* 123 (2000) 281–307. DOI: 10.1016/S0010-2180(00)00155-3
[27]. R.R. Cao and S.B. Pope, *Combust. Flame* 143 (2005) 450–470. DOI: 10.1016/j.combustflame.2005.08.018
[28]. Y. Ge, M.J. Cleary and A.Y. Klimenko, *P. Combust. Inst.* 34 (1) (2013) 1325–1332. DOI: 10.1016/j.proci.2012.06.059
[29]. K. Vogiatzaki, M.J. Cleary, A. Kronenburg and J.H. Kent, *Phys. Fluids* 21 (2) (2009) 1–11. DOI: 10.1063/1.3081553